Attribution of ionospheric vertical plasma drift perturbations to large-scale waves and the dependence on solar activity

H.-L. Liu[1] and A. D. Richmond[1]

Received 25 October 2012; revised 2 April 2013; accepted 4 April 2013; published 10 May 2013.

[1] In this study, we quantify the contribution of individual large-scale waves to ionospheric electrodynamics and examine the dependence of the ionospheric perturbations on solar activity. We focus on migrating diurnal tide (DW1) plus mean winds, migrating semidiurnal tide (SW2), quasi-stationary planetary wave one (QSPW1), and nonmigrating semidiurnal westward wave one (SW1) under northern winter conditions, when QSPW1 and SW1 are climatologically strong. From thermosphere-ionosphere-mesosphere electrodynamics general circulation model simulations under solar minimum conditions, it is found that the mean winds and DW1 produce a wave two pattern in equatorial vertical $\mathbf{E} \times \mathbf{B}$ drift that is upward in the morning and around dusk. The modeled SW2 also produces a wave two pattern in the ionospheric vertical drift that is nearly a half wave cycle out of phase with that due to mean winds and DW1. SW1 can cause large vertical drifts around dawn, while QSPW1 does not have any direct impact on the vertical drift. Wind components of both SW2 and SW1 become large at middle to high latitudes in the E-region, and kernel functions obtained from numerical experiments reveal that they can significantly affect the equatorial ion drift, likely through modulating the E-region wind dynamo. The most evident changes of total ionospheric vertical drift when solar activity is increased are seen around dawn and dusk, reflecting the more dominant role of large F-region Pedersen conductivity and of the F-region dynamo under high solar activity. Therefore, the lower atmosphere driving of the ionospheric variability is more evident under solar minimum conditions, not only because variability is more identifiable in a quieter background but also because the E-region wind dynamo is more significant. These numerical experiments also demonstrate that the amplitudes, phases, and latitudinal and vertical structures of large-scale waves are important in quantifying the ionospheric responses.

Citation: Liu, H.-L., and A. D. Richmond (2013), Attribution of ionospheric vertical plasma drift perturbations to large-scale waves and the dependence on solar activity, *J. Geophys. Res. Space Physics*, *118*, 2452–2465, doi:10.1002/jgra.50265.

1. Introduction

[2] Ionosphere-thermosphere (IT) variability is ubiquitous, and a better understanding of the causes of the variability is an important goal in the study of the space environment. Perturbations from the lower atmosphere are probably an important driver of IT variability. According to the estimate by *Rishbeth and Mendillo* [2001], lower atmosphere driving could make contributions to day-to-day F2 region variability comparable to geomagnetic forcing under moderate solar conditions. Atmosphere waves are capable of vertically transferring momentum and energy from the lower to the upper atmosphere, and the wave amplitudes can be large in the IT region, where the air density is small. The dominant large-scale waves in the IT system are solar thermal tides, which are generated from tropospheric long-wave radiative heating, latent heat release, and stratospheric short-wave (ozone) radiative heating [e.g., *Chapman and Lindzen*, 1970; *Forbes*, 1995; *Hagan and Forbes*, 2002, 2003]. These tides have been used to explain observed temperature and density perturbations in the thermosphere [e.g., *Akmaev et al.*, 2009; *Miyoshi et al.*, 2009; *Akmaev et al.*, 2010; *Lei et al.*, 2011]. Tides can also affect the ionosphere by perturbing the wind dynamo and plasma/neutral transport [e.g., *Richmond and Roble*, 1987; *Fesen et al.*, 2000; *Millward et al.*, 2001]. The observed four-peak longitude structure in the equatorial ionospheric anomaly (EIA) is thought to be a signature of nonmigrating diurnal eastward propagating wave three tide [*Sagawa et al.*, 2005; *Immel et al.*, 2006; *Hagan et al.*, 2009; *Wan et al.*, 2008]. Various nonmigrating tides have also been shown to propagate into the upper thermosphere [e.g., *Häusler et al.*, 2010].

[1]High Altitude Observatory, National Center for Atmospheric Research, Boulder, Colorado, USA.

Corresponding author: H.-L. Liu, High Altitude Observatory, National Center for Atmospheric Research PO Box 3000, Boulder, CO 80307-3000, USA. (liuh@ucar.edu)

2169-9380/13/10.1002/jgra.50265

[3] Traveling planetary waves (TPWs) have been thought to be another driver of ionospheric variability, because the latter often displays periodicities that coincide with the TPW periods [e.g., *Ito et al.*, 1986; *Pancheva and Lysenko*, 1988; *Laštovička and Pancheva*, 1991; *Chen*, 1992; *Canziani*, 1994a; *Altadill and Apostolov*, 2001; *Haldoupis et al.*, 2004; *Fagundes et al.*, 2005; *Xiong et al.*, 2006; *Chang et al.*, 2011; *Liu et al.*, 2012]. Although some of the ionospheric oscillations with periods that are subharmonics of 27 days have been shown to be caused by solar coronal holes and high-speed solar wind streams [*Lei et al.*, 2008], TPWs are still a viable mechanism for producing IT variability. For example, ultra-fast Kelvin waves can penetrate to the middle thermosphere and have been shown numerically and observationally to cause thermospheric density variations of ∼10%, and total electron content (TEC) variations of 10–15% during the day and 15–20% at night [*Forbes*, 2000; *Takahashi et al.*, 2007; *Chang et al.*, 2010; *England et al.*, 2012]. The quasi-2 day wave (QTDW) is a large recurring wave in the mesosphere and lower thermosphere and has been extensively studied observationally, analytically, and numerically. The QTDW causes large wind perturbations in the mesosphere/mesopause region and in the equatorial lower thermosphere [*Wu et al.*, 1993; *Ward et al.*, 1996; *Limpasuvan et al.*, 2005; *Niciejewski et al.*, 2011], with a large mesosphere/mesopause amplitude due primarily to wave amplification from baroclinic/barotropic instability near the summer mesopause and a large equatorial lower thermosphere amplitude due to vertical propagation and amplitude growth under favorable wind conditions and/or possible gravity wave forcing [*Plumb*, 1983; *Palo et al.*, 1999; *Liu et al.*, 2004; *Yue et al.*, 2012a]. Likewise, a quasi-2 day oscillation (QTDO) of the ionosphere is sometimes a prominent feature, and its possible connection with QTDW has been suggested by observational and statistical studies [*Ito et al.*, 1986; *Chen*, 1992; *Canziani*, 1994a; *Forbes et al.*, 1997; *Forbes and Zhang*, 1997; *Gurubaran et al.*, 2001; *Takahashi et al.*, 2005; *Pancheva*, 2006; *Pancheva et al.*, 2006; *Pedatella and Forbes*, 2012]. In particular, *Pancheva et al.* [2006] examined the longitude wave numbers and amplitudes of neutral atmosphere QTDW in mesosphere/lower thermosphere and QTDO in geomagnetic perturbations, and found that, although the wave numbers of the two might not be inconsistent with each other during the observation period, the amplitude increase of QTDO does not seem to correspond to QTDW change. They proposed that nonlinear modulation of tides by QTDW might play an important role in causing geomagnetic QTDO. Using thermosphere-ionosphere-mesosphere electrodynamics general circulation model (TIME-GCM) simulations, *Yue et al.* [2012b] demonstrated that QTDW winds perturb the E-region dynamo and thereby the F-region plasma density, total electron content (TEC), and the equatorial ionospheric anomaly (EIA). Modulation of tidal amplitude by QTDW is not evident in their numerical simulations.

[4] Quasi-stationary planetary waves (QSPWs) are the most dominant planetary waves in the winter stratosphere and mesosphere. Apart from causing perturbations of the temperature and wind (and thus of the polar vortex), they exert westward forcing on the mean flow and drive a poleward circulation in the stratosphere. The QSPWs are usually confined to middle to high latitudes below the winter mesopause by critical layers formed by wind reversal, though forcing by filtered gravity waves may cause in situ generation of QSPWs in the winter thermosphere at high latitudes [*Smith*, 1997]. Under favorable conditions, the QSPWs (most often waves one and two) and their westward forcing can dramatically increase in a short period of time, slow down, or even reverse the winter stratospheric jet, enhance the poleward circulation, and cause large adiabatic heating in the downward branch of the circulation cell. This is the mechanism proposed by *Matsuno* [1971] to explain the stratospheric sudden warming (SSW), first discovered observationally by *Scherhag* [1952]. The weakening/reversal of the stratospheric jet allows more eastward gravity waves to propagate into the mesosphere and lower thermosphere, where their forcing changes the circulation and thermal structure [*Holton*, 1983; *Liu and Roble*, 2002]. Gravity wave effects up to the upper thermosphere and F-region during SSW are examined by *Yiğit and Medvedev* [2012]. The middle and upper atmosphere wind and thermal structures at lower latitudes and in the opposite hemisphere also show teleconnection patterns during the warm stratospheric anomalies (including but not limited to SSW), probably due to a combination of flow continuity, associated changes of latitudinal temperature gradient (thus thermal winds) at lower latitudes and in the opposite hemisphere, and changes of planetary-wave and gravity-wave propagation and forcing [*Becker and Schmitz*, 2003; *Becker et al.*, 2004; *Becker and Fritts*, 2006; *Karlsson et al.*, 2007, 2009a, 2009b; *Xu et al.*, 2009; *Gumble and Karlsson*, 2011; *Espy et al.*, 2011; *Tan et al.*, 2012]. The temperature in the upper thermosphere may also change during SSW, though it could be challenging to separate the SSW effects from solar and geomagnetic driving [*Liu et al.*, 2011; *Fuller-Rowell et al.*, 2011a].

[5] Both migrating and nonmigrating tides can change, through nonlinear interaction with planetary waves and/or due to mean wind change [*Teitelbaum and Vial*, 1991; *Canziani*, 1994b; *Hagan and Roble*, 2001; *Palo et al.*, 1999; *Liu and Roble*, 2002; *Liu et al.*, 2007; *Chang et al.*, 2009, 2011; *Pedatella et al.*, 2012a]. Correlation analysis by *Lieberman et al.* [2004] suggests that the most prominent nonlinear interaction between QSPW1 and the diurnal migrating tide is occurring in the upper stratosphere/lower mesosphere, where QSPW1 peaks. Such changes are important for understanding short-term IT variability, including the variability during SSWs. Mounting observational evidence indicates that the ion and electron temperatures, TEC, ion drifts, EIA, and current system are perturbed during SSWs, and these perturbations often bear tidal periods, suggesting changes in tidal amplitudes and phases [e.g., *Goncharenko and Zhang*, 2008; *Chau et al.*, 2009; *Goncharenko et al.*, 2010a, 2010b; *Yue et al.*, 2010; *Pancheva and Mukhtarov*, 2011; *Pedatella and Forbes*, 2010; *Chau et al.*, 2012; *Yamazaki et al.*, 2012b; *Lin et al.*, 2012]. Mechanistic simulation using the TIME-GCM shows that ionospheric vertical drift and plasma density are perturbed, resulting from modulation of the E-region wind dynamo by migrating and nonmigrating tidal changes when a large QSPW1 is introduced under solar minimum conditions [*Liu et al.*, 2010a]. From NOAA Whole Atmosphere Model (WAM) event simulations and National Center for Atmospheric Research (NCAR) Whole Atmosphere

Community Climate Model (WACCM) ensemble simulations, it is found that solar tides, especially the migrating semidiurnal and terdiurnal tides, can change significantly during SSWs and can result in ionospheric changes [*Fuller-Rowell et al*., 2010; *Pedatella et al*., 2012b; *Jin et al*., 2012]. Apart from tidal interaction with mean winds and QSPWs, an ozone increase during SSWs has been suggested to result in a migrating semidiurnal tidal increase [*Wu et al.*, 2011; *Sridharan et al.*, 2012; *Goncharenko et al.*, 2012]. By assimilating weather data in WAM and coupling it to an ionosphere electrodynamics model, *Fuller-Rowell et al.* [2011b] have been able to produce vertical drift changes that are comparable with ionospheric observations during the 2009 SSW event.

[6] In addition to changes of solar tides, strong signatures of the lunar semidiurnal tide have been identified in the ionospheric equatorial electrojet and vertical drift [*Fejer et al.*, 2010, 2011; *Park et al.*, 2012; *Yamazaki et al.*, 2012a] and in thermospheric temperature and density [*Forbes and Zhang*, 2012] during SSW events. *Stening et al*. [1997] found that the wind and temperature changes in the stratosphere and mesosphere during SSWs could lead to enhancement of the lunar semidiurnal tide from numerical experiments using the Global Scale Wave Model (GSWM). A recent study by Forbes and Zhang (submitted manuscript, 2012) showed that the M2 lunar semidiurnal tide can undergo resonance amplification with wind changes caused by SSW. With the M2 lunar tide included in WACCM and its thermosphere extension (WACCM-X), *Pedatella et al.* [2012b] performed ensemble model simulations and found a statistically significant increase of the M2 tide during SSW. Moreover, by driving the Global Ionosphere-Plasmasphere model [*Millward et al.*, 2001] using thermospheric inputs from WACCM-X, *Pedatella et al.* [2012b] obtained ionospheric vertical drift perturbations that are similar to the observed lunar tidal signature.

[7] It is interesting to note that many observations of the ionospheric responses to lower atmospheric events like SSWs have been reported during the recent solar minimum period. Partly because the ionospheric state is generally quiet relative to periods under more active solar and geomagnetic conditions, it would be easier to identify and isolate signatures from lower atmosphere driving. Even under undisturbed conditions, there are some notable differences between the ionospheric climatology under different solar conditions. For example, ionospheric vertical drifts above Jicamarca display much stronger pre-reversal enhancement (PRE) around dusk, stronger downward drifts at night, weaker upward drifts in the morning, and stronger upward drifts in the afternoon under solar maximum conditions than solar minimum conditions for geomagnetically quiet periods [*Scherliess and Fejer*, 1999]. Consistent with this climatology, observations by the Communication/Navigation Outage Forecasting System (C/NOFS) also show that during the recent extended solar minimum period, vertical drifts can become upward around midnight and around dawn, and downward in the afternoon [*Stoneback et al.*, 2011; *Pfaff et al.*, 2010]. *Stoneback et al.* [2011] suggested that tides may be responsible for these features under solar minimum conditions. *Fejer et al.* [2011] also found stronger ionospheric responses to SSWs under lower solar activity from multiple years of observations, but *Yamazaki et al.* [2012a] found no clear solar activity dependence.

[8] There is clearly a need to better understand and quantify the contribution of each wave component to ionospheric variability, its dependence on the amplitude, phase, and global spatial structure of the wave component, and its dependence on solar activity. A mechanistic study of the ionospheric responses to tides in the presence of a QSPW1 under solar minimum conditions was performed by *Liu et al.* [2010a]. Here we build on that study and attribute the equatorial ionospheric responses to migrating diurnal (plus mean winds), semidiurnal, nonmigrating semidiurnal westward propagating wave one components, and QSPW1. Because the wind perturbations of the migrating and nonmigrating semidiurnal components become large at middle to high latitudes, we further quantify the latitudinal distribution of the wave effects in the equatorial ionosphere. We also examine whether and how the ionospheric responses to these wave perturbations change when solar activity changes. As in *Liu et al.* [2010a], the current study is intended as a mechanistic study to understand the coupling process and various factors that can affect the coupling process. Only a limited but representative set of waves are used to elucidate the analysis and to demonstrate the complex dependence of ionospheric responses on the waves components, their spatial structures, and solar activity.

[9] The TIME-GCM, the design of numerical experiments, and the analysis method are described in section 2. In section 3, we examine the contribution of each wave component to the ionospheric vertical plasma drift (section 3.1), the contribution of semidiurnal tides (migrating and nonmigrating) at different latitudes to the equatorial vertical plasma drift (section 3.2), and the dependence of ionospheric responses to solar activity (section 3.3). Section 4 gives a summary and conclusions.

2. Numerical Experiments and Analysis Method

2.1. Numerical Experiments Using NCAR TIME-GCM

[10] The NCAR thermosphere-ionosphere-mesosphere electrodynamics general circulation model (TIME-GCM) is used for this study. The TIME-GCM is a time-dependent, three-dimensional model that solves the fully coupled, nonlinear, hydrostatic, thermodynamic, and continuity equations of the neutral gas self-consistently from the upper stratosphere to the thermosphere. It combines all previous features of the NCAR thermosphere and ionosphere GCMs, including the self-consistent, fully coupled thermosphere and ionosphere, and electrodynamics driven by the circulation [*Roble et al.*, 1988; *Richmond et al.*, 1992; *Roble and Ridley*, 1994]. The TIME-GCM predicts global winds, temperature, major and minor species composition, electron and ion densities and temperatures, and the ionospheric dynamo electric field. The regular horizontal resolution of the TIME-GCM is 5° × 5°, and the upper boundary of the model for this study is set at 4.6×10^{-10} hPa, two-scale heights higher than the usual upper boundary of the TIME-GCM. There are 49 pressure surfaces from 10 hPa (∼30 km height) to the upper boundary with a vertical resolution of one-half scale height. The input parameters for the TIME-GCM are solar EUV and UV spectral fluxes, parameterized by the solar flux index at 10.7 cm wavelength (F10.7), auroral electron precipitation

by hemispheric power [*Roble and Ridley*, 1987], ionospheric convection driven by the magnetosphere-ionosphere current system [*Heelis et al.*, 1982], and the amplitudes and phases of migrating tides from the lower atmosphere specified by the Global Scale Wave Model (GSWM) [*Hagan et al.*, 1999]. Gravity wave effects are parameterized based on the linear saturation theory of *Lindzen* [1981] up to the lower thermosphere. The details of the model and comparison of model results with observations can be found in *Roble* [2000] and the references therein.

[11] In TIME-GCM simulations, the lower boundary is specified without or with a QSPW perturbation. The base case without QSPW is a climatological simulation for the period of January–March, and the only planetary scale perturbations specified at the lower boundary of the model are migrating tides from GSWM [*Roble*, 2000, and references therein]. In the control case, an idealized QSPW with zonal wave number one is specified at the lower boundary through geopotential height perturbation in addition to the tides. This simulation starts on day number 15, and the amplitude of the QSPW is ramped up using a Gaussian function with a characteristic time of 7 days and peak on day 30. The wave amplitude is kept at the peak value for 10 days before being ramped down using the same Gaussian function. The amplitude of the wave is specified over northern latitudes, with the geopotential height perturbation peaking at 60°N (2500 m during day 30–40). This is somewhat larger than the climatological wave amplitude at this altitude. The reason for using this large wave amplitude is to counter the unrealistic decay of the forced waves near the lower boundary in TIME-GCM. It should be noted that to introduce more realistic meteorological forcing in specific case studies; specification of lower boundary condition could be problematic. Constraining the model over a range of altitudes is needed, as discussed by *Liu et al.* [2013]. The phase of the wave is somewhat arbitrarily set to 140°W. The F10.7 index is set at 70 sfu (solar flux unit), and the geomagnetic activity is low, with the hemispheric power, cross-tail potential, and southward interplanetary magnetic field B_z (inputs to the auroral model and Heelis model) set to 10 GW, 30 kV, and 0, respectively.

2.2. Attribution Method

[12] One purpose of the current study is to quantify the contribution of various wind components to the electric field. The electric potential equation can be written as [*Richmond*, 1983]

$$\nabla \cdot (\boldsymbol{\sigma} \cdot \nabla\Phi) = \nabla \cdot (\boldsymbol{\sigma} \cdot (\mathbf{v} \times \mathbf{B})) = \sum_j \nabla \cdot (\boldsymbol{\sigma} \cdot (\mathbf{v_j} \times \mathbf{B})) \quad (1)$$

where $\boldsymbol{\sigma}$ is the electric conductivity tensor, Φ is the electric potential, $\mathbf{v}$ is the neutral wind vector, and $\mathbf{B}$ is the geomagnetic field vector. In the rightmost equation, the wind is decomposed into various components. This decomposition could be spectrally (by wave components) and/or spatially (over altitudes or latitudes), so that we can study the contribution to the electric potential by wind fields from the jth wave component and/or spatial domain

$$\nabla \cdot (\boldsymbol{\sigma} \cdot \nabla\Phi_j) = \nabla \cdot (\boldsymbol{\sigma} \cdot (\mathbf{v_j} \times \mathbf{B})) \quad (2)$$

[13] In order to have $\sum_j \Phi_j = \Phi$, we disregard changes in σ due to the tides by running the model one step forward, using the decomposed winds in the wind dynamo module. We run a base case that includes only zonal mean winds and migrating diurnal tide, and then obtain Φ_j for all other wind components by adding that wind component to the base case, solving for the potential, and then subtracting the base case potential.

2.3. Physical Interpretation of Neutral Wind Impact on Dynamo

[14] The electric field $\mathbf{E}$ is the negative gradient of the potential Φ. The associated $\mathbf{E} \times \mathbf{B}$ plasma drift velocity is $\mathbf{V}^E = -\nabla\Phi \times \mathbf{B}/B^2$. Under the TIME-GCM assumption that geomagnetic-field lines are equipotential, owing to the very large conductivity parallel to $\mathbf{B}$, $\nabla\Phi$ in (1) is therefore equal to $\mathbf{V}^E \times \mathbf{B}$. This has an important implication: If a component of wind velocity $\mathbf{v}_j$ is of a form that satisfies the physical constraints of the $\mathbf{E} \times \mathbf{B}$ velocity, that is, if the component $\mathbf{v}_{j\perp}$ perpendicular to $\mathbf{B}$ is practically constant along $\mathbf{B}$ and divergence-free (apart from variations along field lines due to variations of $\mathbf{B}$), then a solution of (2) is simply $\mathbf{V}^E = \mathbf{v}_{j\perp}$: The plasma drift velocity equals the component of wind velocity perpendicular to $\mathbf{B}$. This would require uniformity of $\mathbf{v}_{j\perp}$ not only along field lines within the ionosphere of one hemisphere but also between conjugate hemispheres. Although thermospheric winds do not in general satisfy such constraints, there is nonetheless a tendency for the plasma drift velocity partially to follow the wind, in particular the field line-averaged wind as weighted by the Pedersen conductivity. The condition that $\mathbf{V}^E$ must be approximately divergence-free means that the plasma drift velocity cannot entirely follow a wind whose component perpendicular to $\mathbf{B}$ has divergent or convergent regions. In this case, plasma velocities beyond the wind region will be influenced, in order to attain a pattern of $\mathbf{V}^E$ that is divergence-free overall. In particular, the influence of poleward or equatorward midlatitude winds can extend to the magnetic equatorial region, producing poleward/upward or equatorward/downward plasma drifts there.

3. Analysis and Discussion

3.1. Contribution of Wave Components to Ionosphere Plasma Drift

[15] We first examine the contribution of various wave components to the dynamo electric fields. The winds are first decomposed into the most prominent components, which in the current, numerical experiments are the zonal mean, migrating diurnal (DW1), semidiurnal (SW2), nonmigrating semidiurnal westward propagating wave one (SW1), and QSPW1. The sources of the tidal components include forcing at the TIME-GCM lower boundary as well as diurnally varying solar heating of the ozone layer and of the thermosphere. Nonlinear interactions of the tides with the QSPW1 are important, especially for the generation of the SW1 component. Because the role of mean winds and DW1 (and day-night variation) on the ionospheric dynamo is relatively well understood, these two components are not considered separately in this analysis, but rather are combined to form a base case, which we call "Background+DW1." Figure 1 shows the vertical component of the $\mathbf{E} \times \mathbf{B}$ drift (referred to as vertical drift in this paper) at the geographic equator (2.5°N) from these experiments. The mean and DW1 winds

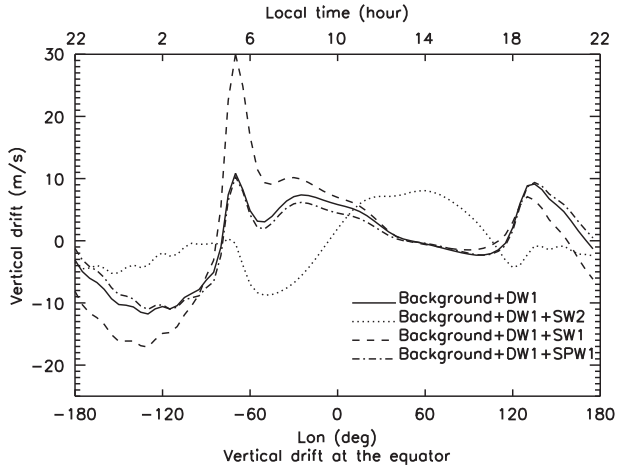

Figure 1. Vertical plasma drifts at 2.5°N and UT1000 on day 31 from TIME-GCM simulations with mean winds and DW1 (solid line); mean winds, DW1 and SW2 (dotted line); mean winds, DW1 and SW1 (dashed line); and mean winds, DW1 and QSPW1 (dash dotted line).

cause upward vertical drift between dawn and ∼LT 1400 and also around dusk, and downward drift in the afternoon and around midnight (∼LT 2200 to 0400). The magnitude of the upward drift goes up to about 10 ms^{-1} at both dawn and dusk, and the downward drift at night can also reach 10 ms^{-1}, while it is weak in the afternoon. The late-morning upward drift is much smaller than the solar-minimum climatologies presented by *Scherliess and Fejer* [1999] and *Stoneback et al.* [2011], which peak around 20 ms^{-1}. Since those climatologies differ considerably in the afternoon and at night, we do not have a clear observational reference for the entire day.

[16] When SW2 is added to the wind, the vertical drift becomes downward in the morning and upward in the afternoon (dotted line in Figure 1). At dusk and in the evening, the vertical drift is rather weak. These changes indicate that the semidiurnal migrating tide in the model produces vertical drifts that are out of phase with those caused by the mean and DW1 winds. It is noteworthy that in the model, SW2 acts to suppress the pre-reversal enhancement (PRE) caused by mean and DW1 winds. Although the addition of the SW2 winds slightly increases the magnitude of the peak upward drift at day, the magnitude of this peak is still much smaller than that seen in the climatologies of *Scherliess and Fejer* [1999] and *Stoneback et al.* [2011], and the peak occurs about 3 h later than in the climatologies. This is probably caused by an incorrect representation of the SW2 phase in the thermosphere. By comparing with the SW2 phase determined from measurements by the Wind Imaging Interferometer (WINDII) [*McLandress et al.*, 1996], it is found that the model SW2 phase lags the observation by 2–4 h between 100–110 km at 35°S (and the SW2 amplitude is underestimated by the model). Nonetheless, the modeled effects of the SW2 on the ionosphere can illustrate qualitatively possible influences of this tide. When SW1 is included along with mean and DW1 winds, there is an upward vertical drift change between LT 0400 and 1200 and a downward change between LT 1700 and 0400. The upward change peaks around dawn (70°W), with an upward drift reaching 30 ms^{-1}; and the downward change peaks at LT 0100 (130°W), with a downward drift of 17 ms^{-1}. So at this UT (1000), the SW1 enhances the vertical drift caused by DW1. It should be noted that because SW1 is a nonmigrating component, its relative phase will be different from the migrating components at different universal times, as can be seen from Figure 4 of *Liu et al.* [2010a]. It is also evident from Figure 1 that in the model, QSPW1 does not contribute to vertical drift change in any significant way.

[17] To further elucidate the contribution from these waves, longitude/latitude maps of vertical drifts caused by mean and DW1 winds, SW2 and SW1 are shown in Figures 2a, 2b, and 2c, respectively. Between 50°S and 50°N, the local time dependence of the vertical drift is quite uniform across latitudes, similar to that at the equator. At dawn, the maximum upward drifts (10–15 ms^{-1}) are located on both sides of the magnetic equator, and the PRE peaks at the magnetic equator. Considering the weak downward drift in the afternoon sector, the vertical drift from mean and DW1 winds displays a wave number two structure in longitude. The SW2 component also produces a wave number two structure in vertical drift (Figure 2b), but the phase is opposite to that due to DW1 at most longitudes: downward in the morning sector and around dusk, and upward in the afternoon and around midnight. The peaks of the vertical drift perturbation due to SW2 track the geomagnetic equator, with amplitude between 10 and 15 ms^{-1}. It is noted that the SW2 component in the equatorial vertical drift peaks at LT 0200/LT 1400. This is similar to the recent

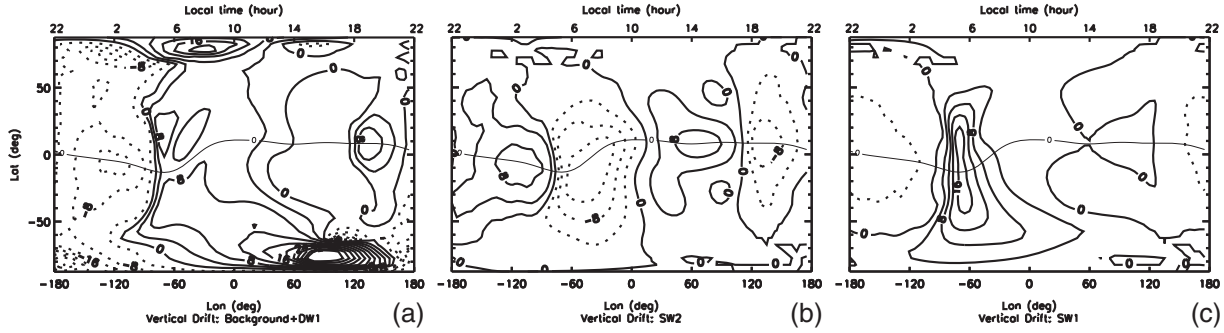

Figure 2. Vertical plasma drifts at UT1000 on day 31 from TIME-GCM simulations with (a) mean winds and DW1, (b) SW2 only, and (c) SW1 only. Contour intervals: 4 ms^{-1}. Solid line: upward drift.

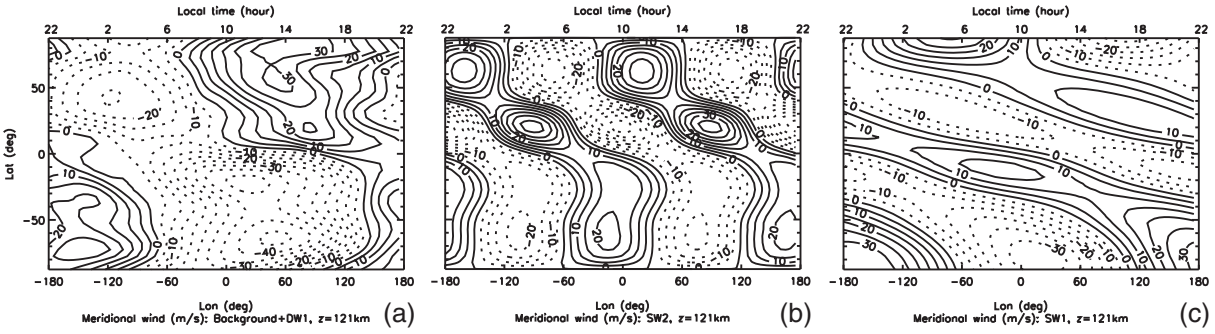

Figure 3. Meridional wind components at ∼121 km and UT1000 on day 31 from TIME-GCM simulations: (a) mean and DW1, (b) SW2, and (c) SW1. Contour intervals: 5 ms^{-1}. Solid line: northward drift.

tidal decomposition study of TEC from the Constellation Observing System for Meteorology, Ionosphere and Climate (COSMIC) measurements by *Chang et al*. [2013]. They found that the equatorial ionosphere anomaly (EIA) has a large SW2 component, and the phase of the EIA is LT 0100–0200 at longitudes where the EIA is strong. Because the rate of development of the EIA is closely tied to the equatorial vertical drift, the EIA strength tends to be strongly related to the vertical drift, with a 1–2 h lag [*Stolle et al.*, 2008; *Jose et al.*, 2011]. The observed timing of the EIA strength again suggests that the phase of the modeled SW2 winds may be 1–3 h later than the actual winds. Additional sensitivity experiments have been performed where the amplitude and phase of SW2 are altered. Doubling of SW2 amplitude at the lower boundary leads to enhanced responses in the vertical drift, although the SW2 amplitude increase is nonuniform in latitude or in altitude, probably due to the varying wind and temperature background. And when the phase of SW2 tidal winds is shifted, the phase of the vertical drift perturbations shifts accordingly (not shown). Therefore, the vertical drift perturbations depend sensitively on the amplitude and phase of SW2, as expected from the linear dependence of wind electric potential on the neutral winds (equation (1)).

[18] The vertical drift perturbation caused by SW1 is most prominent around dawn, with upward drift between LT 0400 and noon. It also causes weak downward drift at low to midlatitudes in early afternoon, and then stronger downward drift between 50°S and 50°N after LT 1800. At dawn, the upward drift can reach 18 ms^{-1}, and it peaks on both sides of the magnetic equator. It also extends well into high southern latitudes.

[19] As found by *Liu et al.* [2010a], both zonal and meridional winds in the ionospheric E-region contribute to the perturbations of vertical ion drift when a planetary wave is introduced. Figure 3 shows the meridional winds of the mean and DW1 component and of the SW2 and SW1 components at ∼121 km, where both the Hall and Pedersen conductivities are large. The winds due to DW1 are poleward during the day and equatorward at night. The SW2 amplitude is larger in the northern hemisphere, and its phase displays a poleward-westward tilt in the winter hemisphere and is approximately constant in latitude (at any given longitude) in the summer hemisphere. This agrees with the SW2 structure from the Global Scale Wave Model (GSWM) [*Hagan et al.*, 1999]. SW2 from the TIMED Doppler Interferometer (TIDI) measurement also shows a larger amplitude in the northern winter hemisphere and phase shift to earlier local times from the southern hemisphere to the northern hemisphere at December solstice [*Wu et al.*, 2011]. The detailed SW2 phase structure from TIDI is quite complex and varies from year to year. In most years, the phase in the lower thermosphere is uniform over southern latitudes, and more variable over equatorial and northern latitudes. At ∼121 km, the model SW2 meridional winds in the summer hemisphere and winter hemisphere up to ∼40°N are equatorward roughly from sunrise to noon and in the evening, and poleward from midnight to dawn and in the afternoon. As discussed in the previous section, winds in the region of considerable Pedersen conductivity have a tendency to drag the ionospheric plasma along through the $\mathbf{E} \times \mathbf{B}$ drifts they generate. As a consequence, the daytime equatorward winds tend to produce equatorward/downward meridional plasma motions at low latitudes, while the daytime poleward winds tend to produce poleward/upward plasma motions at low latitudes. This at least partially contributes to the out of phase behavior of vertical drifts seen in Figure 2.

3.2. Contributions to Ionosphere Plasma Drift From Waves With Large Amplitudes at Higher Latitudes

[20] The SW2 winds maximize at middle to high latitudes, as seen in Figure 3, and so does the change of SW2 when the QSPW is introduced [*Liu et al*., 2010a, Figure 1]. The SW1 meridional winds are also strongest at high latitudes, especially in the summer hemisphere. Similar features were found in a study by *Chang et al.* [2009] examining wave variability during the 2002 southern hemisphere SSW. Because previous works have mainly focused on contribution of atmospheric waves to the ionospheric dynamo at equatorial latitudes, it is worth examining the contributions from waves with large magnitudes at higher latitudes (e.g., SW2 and SW1). And since the SW2 and SW1 winds are asymmetric with respect to the equator, it is also desirable to discern the contributions by the waves from the northern and southern hemispheres.

[21] To quantify the contributions, single step TIME-GCM simulations are made by introducing the winds from a specific wave component (SW2 or SW1) at only one latitude for each simulation. The simulations are repeated for all latitudes. Zonal mean and DW1 winds are included in all the simulations, but their contribution to the electric field is

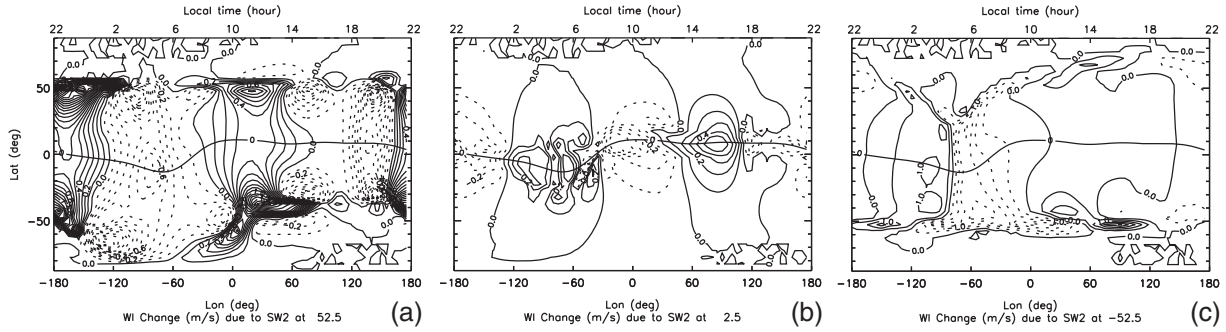

Figure 4. Vertical drift perturbations due to SW2 winds introduced at (a) 52.5°N, (b) 2.5°N, and (c) 52.5°S. The vector winds of SW2 at these latitudes are also plotted. Contour intervals: 0.1 ms^{-1} in Figures 4a and 4b, 0.5 ms^{-1} in Figure 4c.

then subtracted out. From these simulations, we can numerically obtain the kernel function for determining the effects of winds at each latitude on the vertical drift change at specific latitudes (e.g., at the equator).

[22] Figures 4a–4c show the vertical drift perturbations caused by SW2 winds at 52.5°N, 2.5°N, and 52.5°S. By comparison of these three plots, it is clear that the SW2 winds at 52.5°S cause the largest general responses, reaching 1 ms^{-1} (upward) and 1.5 ms^{-1} (downward) near the geographic equator, while the vertical drifts from the SW2 wind at the equator are the weakest. The phases of the vertical drift perturbations from SW2 winds at these latitudes are also different. The vertical drift perturbations due to winds at 52.5°S are largest around dawn: upward between ∼2300 and 0500 LT (170–90°W) and downward between ∼0500 and 1000 LT (90°W–0). The vertical drift perturbations due to winds at the equator, on the other hand, display a clear semidiurnal/wave number two pattern, with upward drifts between ∼0200–0700 LT (120–45°W) and ∼1300–1800 LT (45–120°E) and downward drifts at other local times (longitudes). The SW2 winds at 52.5°N also cause a semidiurnal/wave number two pattern in the vertical drift perturbations, with different phases: upward drifts between ∼2100–0200 LT (165°E–120°W) and ∼0700–1400 LT (45°W–60°E), and downward at other local times (longitudes).

[23] The contribution to the equatorial vertical drift perturbations from SW2 winds at each latitude is more compactly shown in Figure 5. The *y* axis in the plot is the latitude where SW2 winds are turned on in the dynamo solver (set to zero at other latitudes), and the equatorial vertical drift caused by the SW2 winds at this specific latitude is plotted in the figure. The total equatorial vertical drift at any longitude (local time) is just the sum of the values taken at 5° latitude steps for that longitude (5° being the TIME-GCM latitude grid spacing). The semidurnal/wave number two structures in the vertical drift contribution are most visible on both sides of the magnetic equator, with peaks located at 20–40° magnetic latitudes. The largest contribution to the vertical drift comes from SW2 winds at ∼50°S (about 40°S magnetic latitude) near dawn (South America sector). At a specific longitude, the contribution to the vertical drift perturbation from different geographic latitudes may be mutually enhancing or weakening, indicating the intricate dependence on the amplitude, phase, and hemispheric asymmetry of SW2.

[24] As mentioned earlier, the largest wind components of SW1 occur at high latitudes, especially in the summer hemisphere in our numerical experiments. In particular, the maximum meridional wind amplitude is at or near the poles, so that SW1 constitutes a strong cross-polar flow: the flow poleward of ∼40°S crosses from the dayside into the nightside over the South Pole, and the flow poleward of ∼60°N from the dawnside to the duskside over the North Pole. The southern-hemisphere SW1 meridional wind is generally in phase with the DW1 meridional wind. This fact, along with the in-phase relation between the drifts from DW1 and SW1, suggests that SW1 reinforces the DW1 influences on the E-region wind dynamo in this simulation at this universal time. It also suggests that the contribution comes mainly from winds at middle to high latitudes (especially in the southern hemisphere where the SW1 winds are stronger, according to Figure 3c), given that the meridional and zonal winds of SW1 are relatively weak at low latitudes.

[25] Figures 6a–6c show the vertical drift perturbations caused by SW1 winds introduced at 52.5°N, 2.5°N, and 52.5°S. It is clear that SW1 winds at 52.5°S cause the largest global responses. Locally, at 52.5°S, the vertical drift can increase by several meters per second. At lower

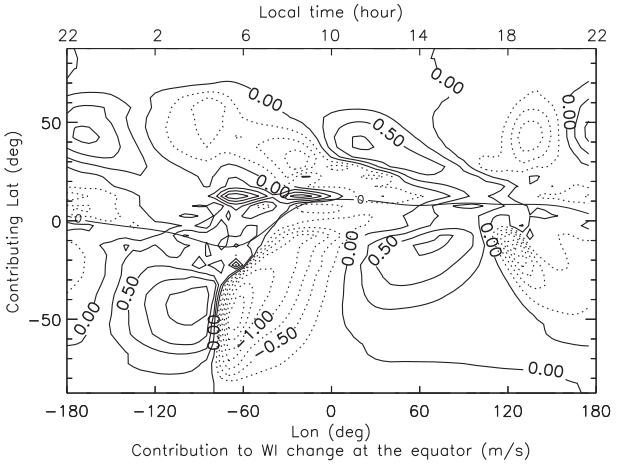

Figure 5. Contribution to the equatorial vertical drift perturbations from SW2 winds at all geographic latitudes. Contour intervals: 0.25 ms^{-1}. Solid line: upward drift contribution.

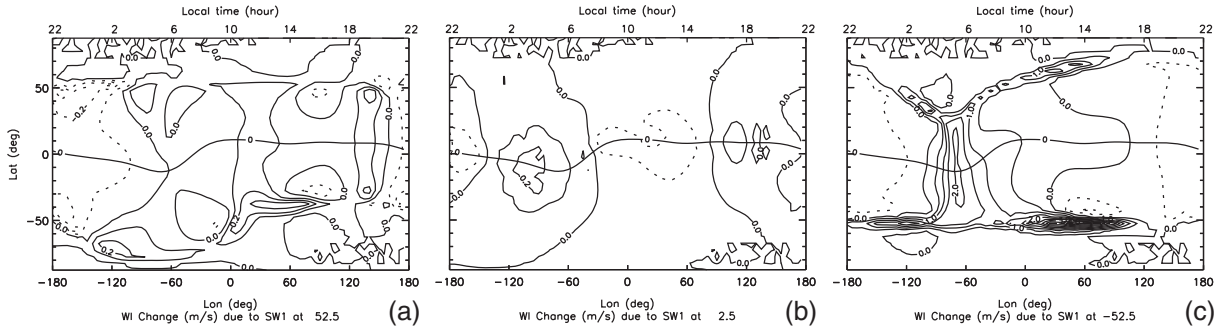

Figure 6. Similar to Figure 4, but for SW1 component.

latitudes, the increase of vertical drift in the upward direction reaches 2 ms^{-1} in the early morning sector. The vertical drifts also change at higher northern latitudes, at the geomagnetic conjugate points of the winds at 52.5°S. The vertical drift magnitudes at the northern conjugate points appear smaller than those in the south due to interpolation of the electric potential from the geomagnetic grid to the northern geographic grid points in the TIME-GCM. The vertical drift perturbations by winds from 52.5°N and 2.5°N are much smaller (0.2–0.3 ms^{-1}). This probably results from a combination of the strong winds and large conductivities in the Southern Hemisphere. The latitudinal distribution of the contribution to the vertical drift change at the equator is shown in Figure 7. It is evident from this plot that the main contribution to the vertical drift perturbations at the equator is from wind dynamo processes associated with SW1 poleward of 30°S. The largest upward drift contribution of about 2.25 ms^{-1} is between LT 0500 and 0600 at 60°S, and the largest downward drift contribution of 1 ms^{-1} is found around midnight between 50 and 60°S. The drift contribution displays a westward tilt and a wave number one structure, consistent with the SW1 winds. In particular, the zero vertical drift generally tracks the zero meridional wind of SW1 (Figure 3), with upward/downward drifts corresponding to poleward/equatorward flows.

[26] From comparing Figure 5 with Figure 3b and Figure 7 with Figure 3c, it is clear that the poleward winds tend to produce poleward/upward $\mathbf{E} \times \mathbf{B}$ drifts that extend to the magnetic equator due to the incompressibility of $\mathbf{E} \times \mathbf{B}$ flow, and that equatorward winds tend to produce equatorward/downward drifts. These results suggest that Pedersen currents associated with the E-region wind dynamo at higher latitudes may play an important role in modulating the electric field and ion drifts at low latitudes. We already discussed how the plasma drifts have a tendency to follow the wind in the region of large Pedersen conductivity, and how the drifts can extend beyond the wind region all the way to the magnetic equator in order to maintain divergence-free plasma flow. Another way to consider this effect is in terms of Pedersen currents and the polarization electric fields they induce. Poleward/equatorward winds can induce westward/eastward Pedersen currents and thus polarization electric fields in the opposite directions (i.e., eastward/westward electric fields). These changes in electric field can map down to lower latitudes and modulate the electrodynamics there (as also seen in Figure 6c). It is noted that, while the vertical drift perturbations are usually larger around dawn and dusk [cf. *Liu et al*., 2010a, Figure 4], they are especially large in the early morning around 70°W. The Pedersen currents converge as the meridional wind changes from equatorward to poleward (in the eastward direction) and diverge with the opposite change. Therefore, the buildup of positive polarization charges is stronger in the former case, and the buildup of negative charges is stronger in the latter case. Furthermore, the geomagnetic equator is close to ∼12°S geographic latitude at 70°W. The large wind and wind changes associated with SW1 are thus located at a lower geomagnetic latitudes, where they can affect the equatorial drift more strongly. The fact that near 70°W the ionosphere at 52.5°S is sunlit in January, while the northern magnetic conjugate region is not, means that Pedersen conductivity at the northern conjugate region is too small to short out electric fields generated in the southern hemisphere, allowing these fields to be particularly strong. *Liu et al.* [2010a] also demonstrated how the electric fields can be enhanced around the terminators.

3.3. Dependence on the Solar Activity

[27] The model simulations discussed earlier in this paper and in *Liu et al.* [2010a] are under solar minimum and geomagnetically quiet conditions. To study the dependence of the ionospheric effects of planetary waves (PWs) on solar activity, we conduct numerical experiments under solar maximum conditions. The numerical experiment setups are the same as those described in *Liu et al.* [2010a], except the

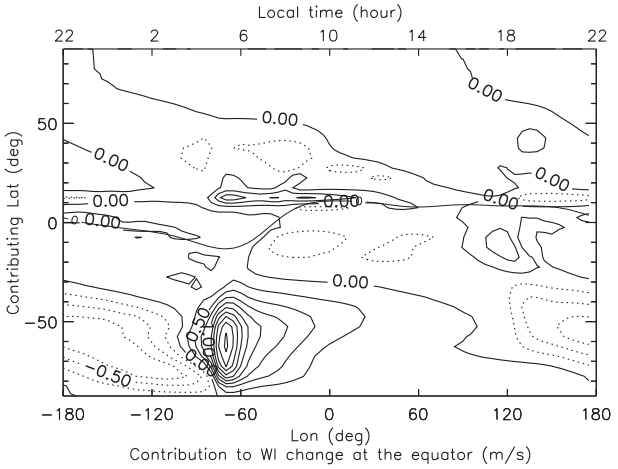

Figure 7. Similar to Figure 5, but for SW1 component.

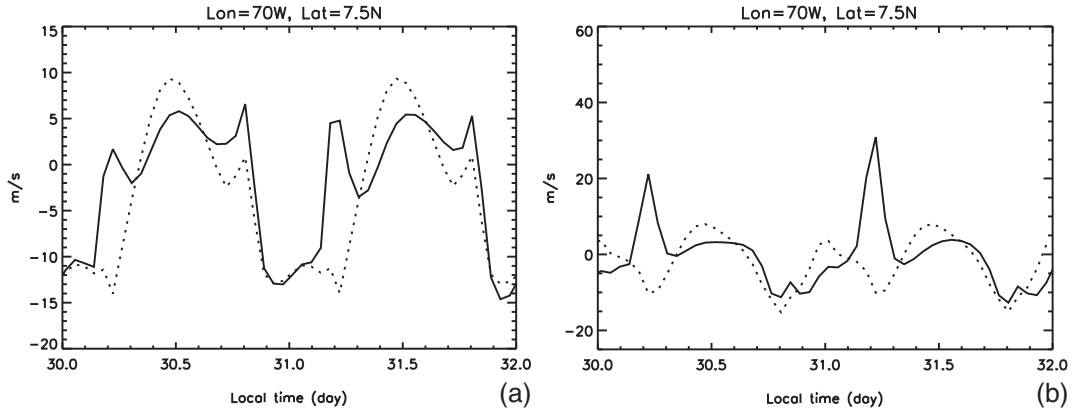

Figure 8. Vertical drifts at 70°W and 7.5°N from simulations under (a) solar maximum and (b) solar minimum conditions without (dotted line) and with (solid line) QSPW1.

F10.7 solar flux index is now set to 200 sfu. The QSPW1 specified at the lower boundary of the model is identical to that used in the earlier experiment. Figure 8 compares the vertical drifts at the equator from the simulations without and with QSPW1 under solar maximum and solar minimum conditions. The change of the vertical drift when the QSPW is introduced displays clear diurnal and semidiurnal periods under both solar conditions, with increases near dawn and dusk, and decreases around noon. The magnitude of the change around dawn to noon, however, is smaller under solar maximum conditions. It is about half of the change in the solar minimum experiment (from ∼40 ms^{-1} to ∼20 ms^{-1} at dawn, and ∼ –10 ms^{-1} to ∼ –5 ms^{-1} at noon). The magnitude of the changes around dusk are similar to those in the solar minimum experiments (5 ms^{-1}). Since the PRE becomes prominent under solar maximum conditions, the vertical drift increases are clearly reflected in the PRE enhancement.

[28] The solar dependence of the ionospheric response to PWs probably reflects primarily the dependence on ionospheric electric conductivities, in particular the F-region Pedersen conductivity. Figure 9 shows the electric conductivities at LT 0500 and 75°W and 2.5°N from the simulations under solar minimum and solar maximum conditions. The peak Pedersen conductivity in the F-region at solar maximum is about four times as large as the value at solar minimum. To further elucidate the dependence of the responses to F-region Pedersen conductivity, single step model simulations are conducted: In the solar minimum simulation, the F-region Pedersen conductivity is increased by fivefold (at altitudes above ∼150 km where σ_P has a minimum at night, Figure 9), while wave characteristics and IT background conditions are exactly the same as in previous numerical experiments. As illustrated in Figure 10, the large equatorial upward vertical drift around dawn is reduced by ∼45 ms^{-1} and becomes downward when the F-region Pedersen conductivity is increased. The vertical drift at dusk, on the other hand, increases by ∼15 ms^{-1}, becomes upward and thus leads to a rather strong PRE. According to Figure 11, the vertical drifts due to DW1, SW2, and SW1 change significantly with the increased Pedersen conductivity: For mean winds and DW1, the downward drift around midnight becomes stronger, and the transition time from downward to upward drift shifts from ∼LT 0430 to LT 0700. Along with this, the rather sharp rise of the vertical drift around LT 0500 has disappeared, and SW1 does not cause any large change of vertical drift around dawn, either. The PRE caused by mean and DW1 winds is twice as strong when the F-region Pedersen conductivity is increased. When SW2 is introduced, the PRE is still quite strong; while according to Figure 1, the vertical drift around dusk is weakly downward in the original solar minimum simulation.

[29] Maps of vertical drift due to mean and DW1, SW2, and SW1 in the simulations with increased F-region Pedersen conductivity are presented in Figure 12. The differences between this figure and Figure 2 are evident. Both the downward drift after LT 2200 and the PRE before LT 2200 due to the mean and DW1 winds are much stronger, while the upward drift in the morning becomes weaker. The vertical drift due to SW2 becomes stronger, except for the upward drift in the evening. And in spite of this general increase, the vertical drift due to SW2 becomes less significant relative to that caused by the mean and DW1 winds around dawn and dusk. The phase of the drift perturbations due to SW2 shifts

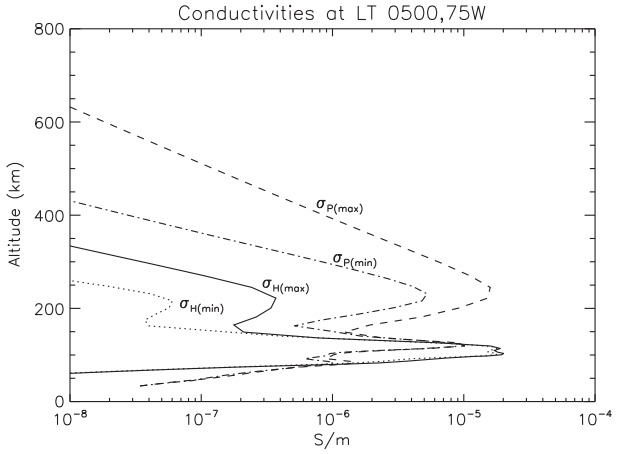

Figure 9. Pedersen and Hall conductivities (σ_P and σ_H, respectively) at LT 0500 h, 75°W and 2.5°N under solar maximum and solar minimum conditions from TIME-GCM.

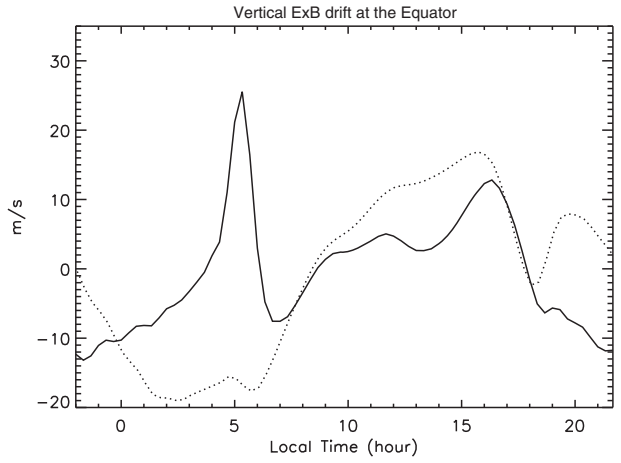

Figure 10. Equatorial vertical drifts from identical TIME-GCM simulations with QSPW1 except the F-region Pedersen conductivity is increased by fivefold (solid line: original σ_p, dotted line: $5\times\sigma_p$).

toward earlier local times by 1–2 h with the increase of the F-region Pedersen conductivity. This is partly responsible for the increase of the total PRE. The drift perturbations due to SW1 become much weaker, particularly in the early morning. This implies a much weaker contribution from the E-region wind dynamo at middle to high latitudes when the F-region Pedersen conductivity is increased.

[30] The opposite changes are seen when the F-region Pedersen conductivity is decreased in a numerical experiment under solar maximum conditions (not shown). All these changes in the experiments with altered F-region Pedersen conductivity are consistent with the changes seen in the numerical experiments when the solar activity is changed. Therefore, solar activity affects the ionospheric responses, in particular at dawn and dusk by changing the F-region Pedersen conductivity. The increase of F-region Pedersen conductivity suppresses the ionospheric responses at dawn, probably by shorting out the E-region dynamo effects, while it enhances the PRE by strengthening the F-region dynamo. With low solar activity, on the other hand, the E-region dynamo effects become more significant. Because they penetrate more readily into the E-region than the F-region, the lower atmosphere waves can exert stronger influence on the ionospheric variability under solar minimum conditions. This may be an additional cause of more evident lower atmosphere signatures in ionospheric variability under solar minimum conditions. It should be noted that the other IT structures changes with solar activity can also affect the propagation of waves. For example, the molecular viscosity decreases with lower solar activity, and the waves originating from the lower atmosphere generally become stronger under solar minimum conditions [*Oberheide et al.*, 2009; *Häusler et al.*, 2010; *Liu et al.*, 2010b].

[31] From climatological studies [e.g., *Scherliess and Fejer*, 1999], the PRE is stronger under solar maximum conditions and weaker under solar minimum conditions. According to *Scherliess and Fejer* [1999], the maximum PRE over Jicamarca is ~60 ms^{-1} and 20 ms^{-1} during geomagnetically quiet periods for November to February under solar maximum and solar minimum conditions, respectively. The maximum downward drift after midnight for these same periods is 50 ms^{-1} and 30–40 ms^{-1}. These features are in qualitative agreement with the solar activity dependence of the vertical drifts induced by mean and DW1 winds identified in the numerical experiments described here, although the magnitudes of the change in the numerical experiments are generally smaller.

[32] Solar activity dependence of ionospheric drifts and their deviation from expected values during the recent extreme solar minimum period are reported from C/NOFS observations [*Stoneback et al.*, 2011; *Pfaff et al.*, 2010]. Under extreme solar minimum conditions (2008–2009), it is found that the vertical drifts at some longitude sectors are upward around midnight and/or dawn and downward in the afternoon. These authors suggested that atmospheric tides may play a key role in these drift changes. Indeed, some of these changes could be interpreted using the understanding gained from the numerical experiments here: with decreasing solar activity, the magnitude of the downward drift around midnight caused by the mean/DW1 winds decreases more significantly than the magnitude of the upward drift by the SW2 winds (Figures 2a–2b and 12a–12b). In the numerical experiments, the mean/DW1/SW2 winds do not quite lead to an upward drift around midnight, but as seen from Figures 1 and 11 the early morning vertical drift is close to zero under solar minimum conditions but strongly downward (~20 ms^{-1}) when σ_P is increased. In the afternoon, the mean/DW1 winds induce weak downward drift under solar minimum conditions (Figure 1) but upward drift when σ_P is increased (Figure 11). The upward vertical drift due to SW2, on the other hand, decreases when σ_P is increased (Figures 2b and 12b). This combination leads to a weaker upward afternoon drift under solar minimum conditions: 8 ms^{-1} at LT 1400 h (compared with 17 ms^{-1} with increased σ_P), and downward after LT 1700 h. This accentuates the important and complex role of the tidal amplitudes, their phases, and their individual dependence on solar activity in determining the ionospheric responses.

[33] As discussed earlier (e.g., Figure 1), both mean/DW1 and SW1 can lead to strong upward drift near dawn under

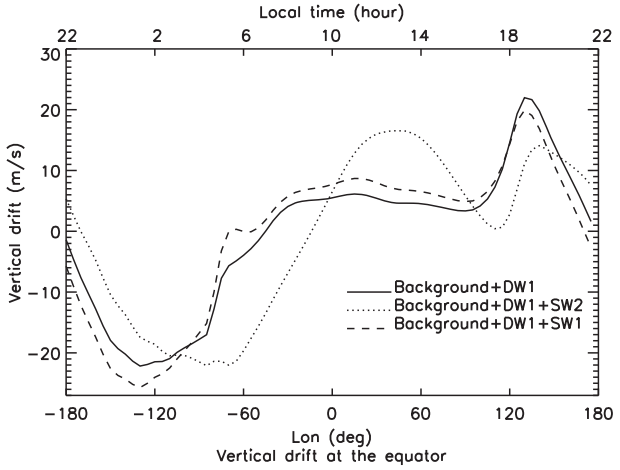

Figure 11. Similar to Figure 1, except the F-region Pedersen conductivity is increased by fivefold.

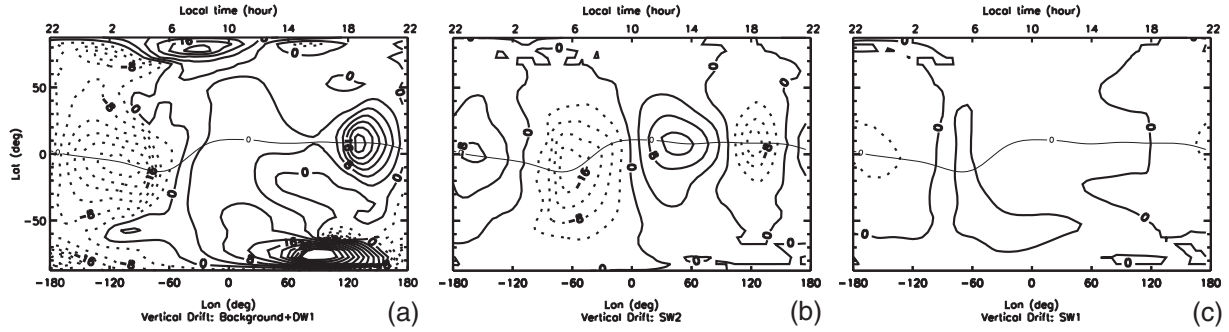

Figure 12. Similar to Figure 2, except the F-region Pedersen conductivity is increased by fivefold.

solar minimum conditions in the numerical simulation. This may explain the large upward drifts seen at dawn as reported by *Stoneback et al.* [2011]. As noted by the authors, such vertical drifts are most noticeable around solstice. This is consistent with the climatology of SW1, which is shown to maximize at solstice [e.g., *Wu et al.*, 2011; *Liu*, 2013], resulting from nonlinear interaction between QSPW1 and SW2. *Stoneback et al.* [2011] also showed that the specific longitude sectors where the upward drift is observed at dawn vary from 1 year to the next. This may reflect the interannual variation of the tidal and planetary wave components (amplitudes and phases). We should also note that the SW1 winds in the control experiments here are stronger than values obtained from observations [*Wu et al.*, 2011].

4. Summary and Conclusions

[34] In this study, we seek to answer the following questions using TIME-GCM: (1) What are the contribution from large-scale waves (planetary waves and tides) to the ionospheric electric dynamo? (2) For wave components that are generally strong at middle and high latitudes, how do they contribute to low latitude electrodynamics? (3) How does solar activity affect the ionospheric responses to these waves? Specifically, we focused on the migrating diurnal tide (DW1, with mean winds), migrating semidiurnal tide (SW2), quasi-stationary planetary wave one (QSPW1), and a nonmigrating tide (SW1, resulting from QSPW1 and SW2 interaction). These waves and their variability are prominent during winter months, especially around stratosphere warming events. Under solar minimum conditions, the mean winds and DW1 produce upward drifts in the morning and around dusk (PRE) and downward drifts in the evening and afternoon, with the latter being very weak in the model (<5 ms^{-1}). The vertical drift due to the modeled SW2 bears a clear wave two pattern and is nearly a half wave cycle out of phase with that due to mean winds and DW1: upward in the afternoon and after midnight, and downward in the morning and around dusk. However, comparisons with observations of vertical drifts in the ionosphere and with the strength of the Equatorial Ionization Anomaly suggest that the phase of the modeled SW2 winds may be retarded with respect to actual thermospheric winds. SW1 induces large a vertical drift around dawn. The largest wind perturbations by SW2 and SW1 occur at middle to high latitudes, and their effects on the equatorial drift are investigated by calculating the kernel function from numerical experiments. The calculation shows that the large wind perturbations at middle and high latitudes can strongly modulate the equatorial vertical drifts through the E-region dynamo, and the net effect is closely tied to the latitudinal and phase structures of these tidal components. The analysis thus demonstrates that superposition of tidal perturbations, their amplitudes, phases, latitudinal/vertical structures, and relative significance are important in determining the ionospheric responses.

[35] The most notable changes when solar activity is increased are around dawn and dusk: The downward drift before dawn is stronger, and the upward drift after dawn and in the morning is weaker; the PRE, on the other hand, becomes stronger. These features are reproduced in the model when F-region Pedersen conductivity is increased, suggesting these changes result from the increasing significance of the F-region dynamo under solar maximum conditions. The longitudinal/local time dependence of the vertical drift due to mean winds and DW1 is similar to that under solar minimum conditions, but there are significant changes in the magnitude of the drift: The downward drift around midnight and the upward drift around dusk (PRE) become much stronger, the upward drift in the morning become weaker, and the drift in the afternoon undergoes an upward change. The vertical drift due to SW2 increases moderately and slightly shifts westward to an earlier local time under solar maximum conditions. Compared with the drift due to mean winds/DW1, the relative significance of SW2 decreases with increasing solar activity around dawn and dusk. The vertical drift caused by SW1 around dawn becomes very weak, suggesting a diminishing role of the E-region wind dynamo at middle to high latitudes under solar maximum conditions. Because the E-region dynamo is more readily modulated by lower atmospheric waves, ionospheric variability is likely to be more affected by these waves under solar minimum conditions than under solar maximum conditions.

[36] The numerical experiments can provide at least a qualitative understanding of some observed equatorial ionospheric features under the recent extreme solar minimum conditions. The observed upward drift around midnight and/or at dawn could be caused by the combination of (1) much weaker downward drift around midnight and much stronger upward drift at dawn due to mean/DW1 winds, (2) upward drift due to SW2 around midnight, and (3) large vertical drift around dawn by SW1 at solstice. At some longitude, the large vertical drift at dawn by SW1 is upward and may explain the observed surge of upward drift by C/NOFS

[*Stoneback et al.*, 2011]. The observed downward drift in the afternoon may result from the combination of downward drift caused by mean/DW1 winds and weaker upward drift by SW2 under extreme solar minimum conditions. The increasing relative significance of SW2 and in general the E-region dynamo also help explain the strong ionospheric responses to lower atmosphere perturbations, such as stratospheric sudden warmings.

[37] **Acknowledgments.** The authors would like to acknowledge valuable discussions with Dr. B. Fejer. This work is in part supported by National Science Foundation Grants ATM-0836386 and AGS-1138784, and NASA LWS NNX08AQ91G and C/NOFS NNX09AN57G. The National Center for Atmospheric Research is sponsored by the National Science Foundation. Robert Lysak thanks the reviewers for their assistance in evaluating this paper.

References

Akmaev, R. A., F. Wu, T. J. Fuller-Rowell, and H. Wang (2009), Midnight temperature maximum (MTM) in Whole Atmosphere Model (WAM) simulations, *Geophys. Res. Lett.*, *36*, L07108, doi:10.1029/2009GL037759.

Akmaev, R. A., F. Wu, T. J. Fuller-Rowell, H. Wang, and M. D. Iredell (2010), Midnight density and temperature maxima, and thermospheric dynamics in Whole Atmosphere Model (WAM) simulations, *J. Geophys. Res.*, *115*, A08326, doi:10.1029/2010JA015651.

Altadill, D., and E. M. Apostolov (2001), Vertical propagating signatures of wave-type oscillations (2- and 6.5-days) in the ionosphere obtained from electron-density profiles, *J. Atmos. Terr. Phys.*, *63*, 823–834.

Becker, E., and D. C. Fritts (2006), Enhanced gravity-wave activity and interhemispheric coupling during the MaCWAVE/MIDAS northern summer program 2002, *Ann. Geophys.*, *24*, 1175–1188.

Becker, E., and G. Schmitz (2003), Climatological effects of orography and land-sea heating contrasts on the gravity wave-driven circulation of the mesosphere, *J. Atmos. Sci.*, *60*, 103–118.

Becker, E., A. Müllemann, F.-J. Lübken, H. Körnich, P. Hoffmann, and M. Rapp (2004), High Rossby-wave activity in austral winter 2002: Modulation of the general circulation of the MLT during the MaCWAVE/MIDAS northern summer program, *Geophys. Res. Lett.*, *31*, L24S03, doi:10.1029/2004GL019615.

Canziani, P. O. (1994a), On tidal variability and the existence of planetary wave-like oscillations in the upper thermosphere 1. Observations of tidal variability, *J. Atmos. Terr. Phys.*, *56*, 901–912.

Canziani, P. O. (1994b), On tidal variability and the existence of planetary wave-like oscillations in the upper thermosphere 2. Nonlinear-interactions and global-scale oscillations, *J. Atmos. Terr. Phys.*, *56*, 913–930.

Chang, L. C., S. E. Palo, and H.-L. Liu (2009), Short-term variation of the s=1 nonmigrating semidiurnal tide during the 2002 sudden stratospheric warming, *J. Geophys. Res.*, *114*, D03109, doi:10.1029/2008JD010886.

Chang, L. C., S. E. Palo, and H.-L. Liu (2010), Response of the thermosphere and ionosphere to an ultra fast Kelvin wave, *J. Geophys. Res.*, *115*, A00G04, doi:10.1029/2010JA015453.

Chang, L. C., S. E. Palo, and H.-L. Liu (2011), Short-term variability in the migrating diurnal tide caused by interactions with the quasi 2 day wave, *J. Geophys. Res.*, *116*, D12112, doi:10.1029/2010JD014996.

Chang, L. C., C.-H. Lin, J.-Y. Liu, N. Balan, J. Yue, and J.-T. Lin (2013), Seasonal and local time variation of ionospheric migrating tides in 2007–2011 FORMOSAT-3/COSMIC and TIE-GCM totel electron content, *J. Geophys. Res. Space Phys.*, *118*, doi:10.1002/jgra.50268.

Chapman, S., and R. S. Lindzen (1970), *Atmospheric, Tides,* 200 pp., D. Reidel Publishing Co., Dordrecht, Holland.

Chau, J. L., B. G. Fejer, and L. P. Goncharenko (2009), Quiet variability of equatorial E×B drifts during sudden stratospheric warming event, *Geophys. Res. Lett.*, *36*, L05101, doi:10.1029/2008GL036785.

Chau, J. L., L. P. Goncharenko, B. G. Fejer, and H.-L. Liu (2012), Equatorial and low latitude ionospheric effects during sudden stratospheric warming events ionospheric effects during SSW events, *Space Sci. Rev.*, *168*, 385–417, doi:10.1007/s11214-011-9797-5.

Chen, P.-R. (1992), Two-day oscillation of the equatorial ionization anomaly, *J. Geophys. Res.*, *97*, 6343–6357.

England, S. L., G. P. Liu, Q. H. Zhou, T. J. Immel, K. K. Kumar, and G. Ramkumar (2012), On the signature of the quasi-3-day wave in the thermosphere during the January 2010 URSI World Day Campaign, *J. Geophys. Res.*, *117*, A06304, doi:10.1029/2012JA017558.

Espy, P. J., S. O. Fernández, P. Forkman, D. Murtagh, and J. Stegman (2011), The role of the QBO in the inter-hemispheric coupling of summer mesospheric temperatures, *Atmos. Chem. Phys.*, *11*, 495–502.

Fagundes, P. R., V. G. Pillat, M. J. A. Bolzan, Y. Sahai, F. Becker-Guedes, J. R. Abalde, S. L. Aranha, and J. A. Bittencourt (2005), Observations of F layer electron density profiles modulated by planetary wave type oscillations in the equatorial ionospheric anomaly region, *J. Geophys. Res.*, *110*, A12302, doi:10.1029/2005JA011115.

Fejer, B. G., M. E. Olson, J. L. Chau, C. Stolle, H. Lühr, L. P. Goncharenko, K. Yumoto, and T. Nagatsuma (2010), Lunar-dependent equatorial ionospheric electrodynamic effects during sudden stratospheric warmings, *J. Geophys. Res.*, *115*, A00G03, doi:10.1029/2010JA015273.

Fejer, B. G., B. D. Tracy, M. E. Olson, and J. L. Chau (2011), Enhanced lunar semidiurnal equatorial vertical plasma drifts during sudden stratospheric warmings, *Geophys. Res. Lett.*, *39*, L21104, doi:10.1029/2011GL049788.

Fesen, C. G., G. Crowley, R. G. Roble, A. D. Richmond, and B. G. Fejer (2000), Simulation of the pre-reversal enhancement in the low latitude vertical ion drift, *Geophys. Res. Lett.*, *27*, 1851–1854.

Forbes, J. M. (1995), Tidal and planetary waves, in *The Upper Mesosphere and Lower Thermosphere: A Review of Experiment and Theory*, edited by R. M. Johnson and T. L. Killeen, 356 pp., no. 87 in Geophysical Monograph Series, Americal Geophysical Union, Washington, D.C.

Forbes, J. M. (2000), Wave coupling between the lower and upper atmosphere: Case study of an ultra-fast, Kelvin wave, *J. Atmos. Solar-Terr. Phys.*, *62*, 1603–1621.

Forbes, J. M., and X. Zhang (1997), Quasi-2-day oscillation of the ionosphere: A statistical study, *J. Atmos. Terr. Phys.*, *59*, 1025–1034.

Forbes, J. M., and X. Zhang (2012), Lunar tide amplification during the January 2009 stratosphere warming event: Observations and theory, *J. Geophys. Res.*, *117*, A12312, doi:10.1029/2012JA017963.

Forbes, J. M., R. Guffee, X. Zhang, D. Fritts, D. Riggin, A. Manson, C. Meek, and R. A. Vincent (1997), Quasi 2-day oscillation of the ionosphere during summer 1992, *J. Geophys. Res.*, *102*, 7301–7305.

Fuller-Rowell, T. J., F. Wu, R. A. Akmaev, and E. Araujo-Pradere (2010), A whole atmosphere model simulation of the impact of a sudden stratospheric warming on thermosphere dynamics and electrodynamics, *J. Geophys. Res.*, *115*, A00G08, doi:10.1029/2010JA015524.

Fuller-Rowell, T. J., R. A. Akmaev, F. Wu, M. Fedrizzi, R. A. Viereck, and H. Wang (2011a), Did the January 2009 sudden stratospheric warming cool or warm the thermosphere? *Geophys. Res. Lett.*, *38*, L18104, doi:10.1029/2011GL048985.

Fuller-Rowell, T. J., H. Wang, R. A. Akmaev, F. Wu, T.-W. Fang, M. Iredell, and A. D. Richmond (2011b), Forecasting the dynamic and electrodynamic response to the January 2009 sudden stratospheric warming, *Geophys. Res. Lett.*, *38*, L13102, doi:10.1029/2011GL047732.

Goncharenko, L., and S.-R. Zhang (2008), Ionospheric signatures of sudden stratospheric warming: Ion temperature at middle latitude, *Geophys. Res. Lett.*, *35*, L21103, doi:10.1029/2008GL035684.

Goncharenko, L., J. Chau, H.-L. Liu, and A. J. Coster (2010a), Unexpected connections between the stratosphere and ionosphere, *Geophys. Res. Lett.*, *37*, L10101, doi:10.1029/2010GL043125.

Goncharenko, L., A. J. Coster, J. Chau, and C. Valladares (2010b), Impact of sudden stratospheric warmings on equatorial ionization anomaly, *J. Geophys. Res.*, *115*, A00G07, doi:10.1029/2010JA015400.

Goncharenko, L., A. J. Coster, R. A. Plumb, and D. I. Domeisen (2012), Impact of sudden stratospheric warmings on equatorial ionization anomaly, *Geophys. Res. Lett.*, *39*, L08101, doi:10.1029/2012GL051261.

Gumble, J., and B. Karlsson (2011), Intra- and inter-hemispheric coupling effects on the polar summer mesosphere, *Geophys. Res. Lett.*, *38*, L14804, doi:10.1029/2011GL047968.

Gurubaran, S., T. K. Ramkumar, S. Sridharan, and R. Rajaran (2001), Signatures of quasi-2-day planetary waves in the equatorial electrojet: Results from simultaneous observations of mesospheric winds and geomagnetic field variations at low latitudes, *J. Atmos. Sol. Terr. Phys.*, *63*, 813–821.

Hagan, M. E., and J. M. Forbes (2002), Migrating and nonmigrating diurnal tides in the middle and upper atmosphere excited by tropospheric latent heat release, *J. Geophys. Res.*, *107*, 4754.

Hagan, M. E., and J. M. Forbes (2003), Migrating and nonmigrating semidiurnal tides in the upper atmosphere excited by tropospheric latent heat release, *J. Geophys. Res.*, *108*, 1062.

Hagan, M. E., and R. G. Roble (2001), Modeling diurnal tidal variability with the, National Center for Atmospheric Research thermosphere-ionosphere-mesosphere-electrodynamics general circulation model, *J. Geophys. Res.*, *106*, 24,869–24,882.

Hagan, M. E., M. D. Burrage, J. M. Forbes, J. Hackney, W. J. Randel, and X. Zhang (1999), GSWM-98: Results for migrating solar tides, *J. Geophys. Res.*, *104*, 6813–6828.

Hagan, M. E., A. Maute, and R. G. Roble (2009), Tropospheric tidal effects on the middle and upper atmosphere, *J. Geophys. Res.*, *114*, A01302, doi:10.1029/2008JA013637.

Haldoupis, C., D. Pancheva, and N. J. Mitchell (2004), A study of tidal and planetary wave periodicities present in midlatitude sporadic E layers, *J. Geophys. Res.*, *109*, A02302, doi:10.1029/2003JA010253.

Häusler, K., H. Lühr, M. E. Hagan, A. Maute, and R. G. Roble (2010), Comparison of CHAMP and TIME-GCM nonmigrating tidal signals in the thermospheric zonal wind, *J. Geophys. Res.*, *115*, D00I08, doi:10.1029/2009JD012394.

Heelis, R. A., J. K.Lowell, and R. W.Spiro (1982), A model of the high-latitude ionsophere convection pattern, *J. Geophys. Res.*, *87*, 6339–6345.

Holton, J. R. (1983), The influence of gravity wave breaking on the general circulation of the middle atmosphere, *J. Atmos. Sci.*, *40*, 2497–2507.

Immel, T. J., E. Sagawa, S. L. England, S. B. Henderson, M. E. Hagan, S. B. Mende, H. U. Frey, C. M. Swenson, and L. J. Paxton (2006), Control of equatorial ionospheric morphology by atmospheric tides, *Geophys. Res. Lett.*, *33*, L15108, doi:10.1029/2006GL026161.

Ito, R., S. Kato, and T. Tsuda (1986), Consideration of an ionospheric wind dynamo driven by a planetary wave with a two-day period, *J. Atmos. Terr. Phys.*, *48*, 1–13.

Jin, H., Y. Miyoshi, D. Pancheva, P. Mukhtarov, H. Fujiwara, and H. Shinagawa (2012), Response of migrating tides to the stratospheric sudden warming in 2009 and their effects on the ionosphere studied by a whole atmosphere-ionosphere model GAIA with COSMIC and TIMED/SABER observations, *J. Geophys. Res.*, *117*, A10323, doi:10.1029/2012JA017650.

Jose, L., S. Ravindran, C. Vineeth, T. Pant, and S. Alex (2011), Investigation of the response time of the equatorial ionosphere in context of the equatorial electrojet and equatorial ionization anomaly, *Ann. Geophysicae.*, *29*, 1267–1275, doi:10.5194/angeo-29-1267-2011.

Karlsson, B., and J H. Körnich (2007), Evidence for interhemispheric stratosphere-mesosphere coupling derived from noctilucent cloud properties, *Geophys. Res. Lett.*, *34*, L16806, doi:10.1029/2007GL030282.

Karlsson, B., C. McLandress, and T. G. Shepherd (2009a), Inter-hemispheric mesospheric coupling in a comprehensive middle atmosphere model, *J. Atmos. Solar Terr. Phys.*, *71*, 518–530.

Karlsson, B., C. E. Randall, S. Benze, M. Mills, V. L. Harvey, S. M. Bailey, and J. M. Russell (2009b), Intra-seasonal variability of polar mesospheric clouds due to inter-hemispheric coupling, *Geophys. Res. Lett.*, *36*, L20802, doi:10.1029/2009GL040348.

Laštovička, J., and D. Pancheva (1991), Changes in the characteristics of planetary waves at 80–100 km over central and southern Europe since 1980, *Adv. Space Res.*, *11*, 31–34.

Lei, J., J. P. Thayer, J. M. Forbes, E. K. Sutton, R. S. Nerem, M. Temmer, and A. M. Veronig (2008), Global thermospheric density variations caused by high-speed solar wind streams during the declining phase of solar cycle 23, *J. Geophys. Res.*, *113*, A11303, doi:10.1029/2008JA013433.

Lei, J., J. M. Forbes, H. L. Liu, X. Dou, X. Xue, T. Li, and X. Luan (2011), Latitudinal variations of middle thermosphere: Observations and modeling, *J. Geophys. Res.*, *116*, A12306, doi:10.1029/2011JA017067.

Lieberman, R. S., J. Oberheide, M. E. Hagan, E. E. Remsberg, and L. L. Gordley (2004), Variability of diurnal tides and planetary waves during, November 1978–May 1979, *J. Atmos. Solar Terr. Phys.*, *66*, 517–528.

Limpasuvan, V., D. L. Wu, M. J. Schwartz, J. W. Waters, Q. Wu, and T. L. Killeen (2005), The two-day wave in EOS MLS temperature and wind measurements during 2004–2005 winter, *Geophys. Res. Lett.*, *32*, L17809, doi:10.1029/2005GL023396.

Lin, J. T., C. H. Lin, L. C. Chang, H. H. Huang, J. Y. Liu, A. B. Chen, C. H. Chen, and C. H. Liu (2012), Observational evidence of ionospheric migrating tide modification during the 2009 stratospheric sudden warming, *Geophys. Res. Lett.*, *39*, L02101, doi:10.1029/2011GL050248.

Lindzen, R. S. (1981), Turbulence and stress owing to gravity wave and tidal breakdown, *J. Geophys. Res.*, *86*, 9707–9714.

Liu, G. P., S. L. England, T. J. Immel, K. K. Kumar, G. Ramkumar, and L. P. Goncharenko (2012), Signatures of the 3-day wave in the low-latitude and midlatitude ionosphere during the January 2010 URSI World Day campaign, *J. Geophys. Res.*, *117*, A06305, doi:10.1029/2012JA017588.

Liu, H., E. Doornbos, M. Yamamoto, and S. T. Ram (2011), Strong thermospheric cooling during the 2009 major stratosphere warming, *Geophys. Res. Lett.*, *38*, L12102, doi:10.1029/2011GL047898.

Liu, H.-L. (2013), WACCM-X simulation of upper atmosphere wave variability, in *Modeling the Ionosphere and Thermosphere System*, edited by J. Huba, R. Schunk, and G. Khazanov, Geophysical Monograph Series, pp. 1–19, Americal Geophysical Union, Washington, D.C., doi:10.1029/2012GM001338. in press.

Liu, H.-L., and R. G. Roble (2002), A study of a self-generated stratospheric sudden warming and its mesospheric/lower thermospheric impacts using coupled TIME-GCM/CCM3, *J. Geophys. Res.*, *107*, doi:10.1029/2001JD001533.

Liu, H.-L., E. R. Talaat, R. G. Roble, R. S. Lieberman, D. M. Riggin, and J.-H. Yee (2004), 6.5-day wave and its seasonal variability in the middle and upper atmosphere, *J. Geophys. Res.*, *109*, D21112, doi:10.1029/2004JD004795.

Liu, H.-L., W. Wang, A. D. Richmond, and R. G. Roble (2010a), Ionospheric variability due to planetary waves and tides for solar minimum conditions, *J. Geophys. Res.*, *115*, A00G01, doi:10.1029/2009JA015188.

Liu, H.-L., V. A. Yudin, and R. G. Roble (2013), Day-to-day ionospheric variability due to lower atmosphere perturbations, *Geophys. Res. Lett.*, *40*, 1–6, doi:10.1002/grl.50125.

Liu, H. L., et al. (2007), Comparative study of short term tidal variability, *J. Geophys. Res.*, *112*, D18108, doi:10.1029/2007JD008542.

Liu, H.-L., et al. (2010b), Thermosphere extension of the whole atmosphere community climate model, *J. Geophys. Res.*, *115*, A12302, doi:10.1029/2010JA015586.

Matsuno, T. (1971), A dynamical model of the stratospheric sudden warming, *J. Atmos. Sci.*, *28*, 1479–1494.

McLandress, C. M., G. G. Shepherd, and B. H. Solheim (1996), Satellite observations of thermospheric tides: Results from the Wind Imaging Interferometer on UARS, *J. Geophys. Res.*, *101*, 4093–4114.

Millward, G. H., I. Muller-Wodarg, A. Aylward, T. Fuller-Rowell, A. Richmond, and R. Moffett (2001), An investigation into the influence of tidal forcing on F region equatorial vertical ion drift using a global ionosphere-thermosphere model with coupled electrodynamics, *J. Geophys. Res.*, *106*, 24,733–24,744.

Miyoshi, Y., H. Fujiwara, J. M. Forbes, and S. L. Bruinsma (2009), Solar terminator wave and its relation to the atmospheric tide, *J. Geophys. Res.*, *114*, A07303, doi:10.1029/2009JA014110.

Niciejewski, R., W. Skinner, M. Cooper, A. Marshall, R. R. Meier, M. H. Stevens, D. Ortland, and Q. Wu (2011), Verification of large-scale rapid transport in the lower thermosphere: Tracking the exhaust plume of STS-107 from launch to the Antarctic, *J. Geophys. Res.*, *116*, A05302, doi:10.1029/2010JA016277.

Oberheide, J., J. M. Forbes, K. Häusler, Q. Wu, and S. L. Bruinsma (2009), Tropospheric tides from 80 to 400 km: Propagation, interannual variability, and solar cycle effects, *J. Geophys. Res.*, *114*, D00I05, doi:10.1029/2009JD012388.

Palo, S. E., R. G. Roble, and M. E. Hagan (1999), Middle atmosphere effects of the quasi-two-day wave determined from a general circulation model, *Earth Planets Space*, *51*, 629–647.

Pancheva, D. V. (2006), Quasi-2-day wave and tidal variability observed over, Ascension Island during January/February 2003, *J. Atmos. Solar Terr. Phys.*, *68*, 390–407.

Pancheva, D. V., and I. Lysenko (1988), Quasi-two-day fluctuations observed in the summer F-region electron maximum, *Bulg. Geophys. J.*, *14*, 41–51.

Pancheva, D. V., and P. Mukhtarov (2011), Stratospheric warmings: The atmosphere ionosphere coupling paradigm, *J. Atmos. Solar Terr. Phys.*, *73*, 1697–1702.

Pancheva, D. V., et al. (2006), Two-day wave coupling of the low-latitude atmosphere-ionosphere system, *J. Geophys. Res.*, *111*, A07313, doi:10.1029/2005JA011562.

Park, J., H. Lühr, M. Kunze, B. G. Fejer, and K. W. Min (2012), Effect of sudden stratospheric warming on lunar tidal modulation of the equatorial electrojet, *J. Geophys. Res.*, *117*, A03306, doi:10.1029/2011JA017351.

Pedatella, N. M., and J. M. Forbes (2010), Evidence for stratosphere sudden warming-ionosphere coupling due to vertically propagating tides, *Geophys. Res. Lett.*, *37*, L11104, doi:10.1029/2010GL043560.

Pedatella, N. M., and J. M. Forbes (2012), The quasi 2 day wave and spatial-temporal variability of the OH emission and ionosphere, *J. Geophys. Res.*, *117*, A01320, doi:10.1029/2011JA017186.

Pedatella, N. M., H.-L. Liu, and M. E. Hagan (2012a), Day-to-day migrating and nonmigrating tidal variability due to the six-day planetary wave, *J. Geophys. Res.*, *117*, A06301, doi:10.1029/2012JA017581.

Pedatella, N. M., H.-L. Liu, A. D. Richmond, A. Maute, and T.-W. Fang (2012b), Simulations of solar and lunar tidal variability in the mesosphere and lower thermosphere during sudden stratosphere warmings and their influence on the low-latitude ionosphere, *J. Geophys. Res.*, *117*, A08326, doi:10.1029/2012JA017858.

Pfaff, R., D. Rowland, H. Freudenreich, K. Bromund, G. Le, M. Acuña, J. Klenzing, C. Liebrecht, and S. Martin (2010), Observations of DC electric fields in the low latitude ionosphere and their variations with local time, longitude, and plasma density during extreme solar minimum, *J. Geophys. Res.*, *115*, A12324, doi:10.1029/2010JA016023.

Plumb, R. A. (1983), Baroclinic instability of the summer mesosphere: A mechanism for the quasi-two-day wave? *J. Atmos. Sci.*, *40*, 262–270.

Richmond, A. D. (1983), Thermospheric dynamics and electrodynamics, in *Solar-Terrestrial, Physics*, edited by R. L. Carovillano and J. M. Forbes, 859 p., no. 104 in Astrophysics and Space Science Library, D. Reidel Publishing Company, Dordrecht/Boston/Lancaster.

Richmond, A. D., and R. G. Roble (1987), Electrodynamic effects of thermospheric winds from the NCAR Thermospheric General-Circulation Model, *J. Geophys. Res.*, *92*, 12,365–12,376.

Richmond, A. D., E. C. Ridley, and R. G. Roble (1992), A thermosphere/ionosphere general circulation model with coupled electrodynamics, *Geophys. Res. Lett.*, *19*, 601–604.

Rishbeth, H., and M. Mendillo (2001), Patterns of ionospheric variability, *J. Atmos. Solar Terr. Phys.*, *63*, 1661–1680.

Roble, R. G. (2000), On the feasibility of developing a global atmospheric model extending from the ground to the exosphere, in *Atmospheric Science Across the Stratopause*, edited by D. E. Siskind, S. D. Eckermann, and M. E. Summers, 342 p., no. 123 in Geophysical Monograph Series, Americal Geophysical Union, Washington, D.C.

Roble, R. G., and E. C. Ridley (1987), An auroral model for the NCAR thermosphere general circulation model (TGCM), *Annales. Geophysicae.*, *5A*, 369–382.

Roble, R. G., and E. C. Ridley (1994), A thermosphere-ionosphere-mesosphere-electrodynamics general circulation model (TIME-GCM): Equinox solar cycle minimum simulations (30–500 km), *Geophys. Res. Lett.*, *21*, 417–420.

Roble, R. G., E. C. Ridley, A. D. Richmond, and R. E. Dickinson (1988), A coupled thermosphere/ionosphere general circulation model, *Geophys. Res. Lett.*, *15*, 1325–1328.

Sagawa, E., T. J. Immel, H. U. Frey, and S. B. Mende (2005), Longitudinal structure of the equatorial anomaly in the nighttime ionosphere observed by IMAGE/FUV, *J. Geophys. Res.*, *110*, A11302, doi: 10.1029/2004JA010848.

Scherhag, R. (1952), Die explosionsartigen stratospärenerwärmungen des spätwinters 1951-1952, *Ber. Dtsch. Wetterdienst (US Zone)*, *6*, 51–63.

Scherliess, L., and B. G. Fejer (1999), Radar and satellite global equatorial F region vertical drift model, *J. Geophys. Res.*, *104*, 6829–6842.

Smith, A. K. (1997), Stationary planetary waves in upper mesospheric winds, *J. Atmos. Sci.*, *54*, 2129–2145.

Sridharan, S., S. Sathishkumar, and S. Gurubaran (2012), Variabilities of mesospheric tides during sudden stratospheric warming events of 2006 and 2009 and their relationship with ozone and water vapour, *J. Atmos. Terr. Phys.*, *78*, 108–115, doi:10.1016/j.jastp.2011.03.013.

Stening, R. J., J. M. Forbes, M. E. Hagan, and A. D. Richmond (1997), Experiments with a lunar atmospheric tidal model, *J. Geophys. Res.*, *102*, 13,465–13,471.

Stolle, C., C. Manoj, H. Lühr, S. Maus, and P. Alken (2008), Estimating the daytime equatorial ionization anomaly strength from electric field proxies, *J. Geophys. Res.*, *113*, A09310, doi:10.1029/2007JA012781.

Stoneback, R. A., R. A. Heelis, A. G. Burrell, W. R. Coley, B. G. Fejer, and E. Pacheco (2011), Observations of quiet time vertical ion drift in the equatorial ionosphere during the solar minimum period of 2009, *J. Geophys. Res.*, *116*, A12327, doi:10.1029/2011JA016712.

Takahashi, H., L. M. Lima, C. M. Wrasse, M. A. Abdu, I. S. Batista, D. Gobbi, R. A. Buriti, and P. P. Batista (2005), Evidence on 2–4 day oscillations of the equatorial ionosphere h'f and mesospheric airglow emissions, *Geophys. Res. Lett.*, *32*, L12102, doi:10.1029/2004GL022318.

Takahashi, H., et al. (2007), Signatures of ultra fast Kelvin waves in the equatorial middle atmosphere and ionosphere, *Geophys. Res. Lett.*, *34*, L11108, doi:10.1029/2007GL029612.

Tan, B., X. Chu, H.-L. Liu, C. Yamashita, and J. M. Russell III (2012), Zonal-mean global teleconnection from 15 to 110 km derived from SABER and WACCM, *J. Geophys. Res.*, *117*, D10106, doi:10.1029/2011JD016750.

Teitelbaum, H., and F. Vial (1991), On tidal variability induced by nonlinear-interaction with planetary-waves, *J. Geophys. Res.*, *96*, 14,169–14,178, doi:10.1029/91JA01019.

Wan, W., L. Liu, X. Pi, M.-L. Zhang, B. Ning, J. Xiong, and F. Ding (2008), Wavenumber-4 patterns of the total electron content over the low latitude ionosphere, *Geophys. Res. Lett.*, *35*, L12104, doi:10.1029/2008GL033755.

Ward, W. E., D. Y. Wang, B. H. Solheim, and G. G. Shepherd (1996), Observations of the two-day wave in WINDII data during January, *Geophys. Res. Lett.*, *23*, 2923–2926.

Wu, D. L., P. B. Hays, W. R. Skinner, A. R. Marshall, M. D. Burrage, R. S. Lieberman, and D. A. Ortland (1993), Observations of the quasi 2-day wave from the high-resolution Doppler imager on UARS, *Geophys. Res. Lett.*, *20*, 2853–2856.

Wu, Q., D. A. Ortland, S. C. Solomon, W. R. Skinner, and R. J. Niciejewski (2011), Global distribution, seasonal, and inter-annual variations of mesospheric semidiurnal tide observed by TIMED TIDI, *J. Atmos. Solar Terr. Phys.*, *73*, 2482–2502, doi:10.1016/j.jastp.2011.08.007.

Xiong, J., W. Wan, B. Ning, L. Liu, and Y. Gao (2006), Planetary wave-type oscillations in the ionosphere and their relationship to mesospheric/lower thermospheric and geomagnetic disturbances at Wuhan (30.61°N, 114.51°E), *J. Atmos. Solar Terr. Phys.*, *68*, 498–508.

Xu, X., A. H. Manson, C. E. Meek, T. Chshyolkova, J. R. Drummond, C. M. Hall, D. M. Riggin, and R. E. Hibbins (2009), Vertical and interhemispheric links in the stratosphere-mesosphere as revealed by the day-to-day variability of Aura-MLS temperature data, *Ann. Geophys.*, *27*, 3387–3409.

Yamazaki, Y., A. D. Richmond, and K. Yumoto (2012a), Stratospheric warmings and the geomagnetic lunar tide: 1958–2007, *J. Geophys. Res.*, *117*, A04301, doi:10.1029/2012JA017514.

Yamazaki, Y., K. Yumoto, D. J. McNamara, T. Hirooka, T. Uozumi, K. Kitamura, S. Abe, and A. Ikeda (2012b), Ionospheric current system during sudden stratospheric warming events, *J. Geophys. Res.*, *117*, A03334, doi:10.1029/2011JA017453.

Yiğit, E., and A. S. Medvedev (2012), Gravity waves in the thermosphere during a sudden stratospheric warming, *Geophys. Res. Lett.*, *39*, L21101, doi:10.1029/2012GL053812.

Yue, J., H.-L. Liu, and L. C. Chang (2012a), Numerical investigation of the quasi 2 day wave in the mesosphere and lower thermosphere, *J. Geophys. Res.*, *117*, D05111, doi:10.1029/2011JD016574.

Yue, J., W. Wang, A. D. Richmond, and H.-L. Liu (2012b), Quasi-two-day wave coupling of the mesosphere and lower thermosphere-ionosphere in the TIME-GCM: Two-day oscillations in the ionosphere, *J. Geophys. Res.*, *117*, A07305, doi:10.1029/2012JA017815.

Yue, X., W. S. Schreiner, J. Lei, C. Rocken, D. C. Hunt, Y.-H. Kuo, and W. Wan (2010), Global ionospheric response observed by COSMIC satellites during the January 2009 stratospheric sudden warming event, *J. Geophys. Res.*, *115*, A00G09, doi:10.1029/2010JA015466.